Wideband, Low Driving Voltage Traveling-Wave Mach–Zehnder Modulator for RF Photonics

Mona Jarrahi, Thomas H. Lee, and David A. B. Miller

***Abstract*—We report the design, fabrication, and testing of a traveling-wave Mach–Zehnder modulator on a GaAs substrate. Operating at 870-nm wavelength, we obtained an extremely low driving voltage of 0.45 V and a high measurement-instrument-limited small-signal modulation bandwidth of 18 GHz, projected to an estimated bandwidth of 50 GHz. We have also monolithically integrated photodetectors with an impulse response of 8-ps full-width at half-maximum, and a saturation power of 330 mW, giving a flexible high-performance platform for RF photonics.**

***Index Terms*—Optical device fabrication, optical modulation, phase modulation, photodetectors, quantum-confined Stark effect (QCSE).**

I. INTRODUCTION

OPTICAL modulators are important components for both high-bit-rate telecommunications [1], [2] and for optical signal processing of high-frequency electromagnetic signals [3]–[6]. Optics offers many benefits for handling analog RF signals, including simplified distribution, low propagation loss, large modulation bandwidths, and the large computational parallelism of optical waves as the information carrier. Low-drive-voltage Mach–Zehnder (MZ) modulators with large modulation bandwidth [7] are particularly important for RF photonics. Additionally, especially for analog systems, the ability to fabricate high-speed photodetectors, capable of operating with high optical powers, on the same substrate with the MZ modulator can be very useful.

In this work, we demonstrate MZ modulators with particularly low voltage for π phase shift $(V\pi)$, while retaining very high electrical modulation bandwidth, and also allowing high-speed photodiodes, linear to high optical powers, to be fabricated in the same structure. We have already been able to demonstrate the application of these integrated devices to analog-to-digital conversion at very high bandwidths [8].

The low modulator drive voltage is achieved by combining a relatively long device length with high electro-refractive effect induced by the quantum-confined Stark effect (QCSE) [9], [10]. By utilizing velocity-matched traveling-wave modulator architecture [11], allowing a long modulation path while maintaining a small junction area, the interdependence of modulation bandwidth and efficiency is reduced.

Manuscript received October 22, 2007; revised December 5, 2007. This work was supported by Stanford University Center for Integrated Systems (CIS), by Texas Instruments, and by Agilent Technologies.

M. Jarrahi and T. H. Lee are with Stanford Microwave Integrated Circuits Laboratory, Department of Electrical Engineering, Stanford University, Stanford, CA 94305-4070 USA (e-mail: mjarrahi@smirc.stanford.edu).

D. A. B. Miller is with Ginzton Laboratory, Department of Electrical Engineering, Stanford University, Stanford, CA 94305-4088 USA.

Color versions of one or more of the figures in this letter are available online at http://ieeexplore.ieee.org.

Digital Object Identifier 10.1109/LPT.2008.918889

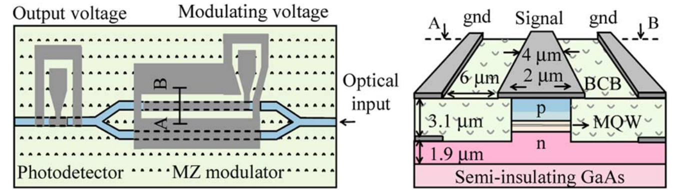

Fig. 1. Schematic of the MZ modulator and the device cross-section.

High photodetector quantum efficiency at the modulator operating wavelength is achieved as a result of the large QCSE-induced absorption edge shift available at large reverse-bias voltages [9]. By employing a relatively long device length, the field screening effect [12] is reduced to further increase the photodetector quantum efficiency. The photodetector length and termination resistance are kept small to achieve high-speed photodetection. For performance optimization of each individual block, we benefit from voltage-controllable electro-refraction induced by the QCSE.

II. MZ MODULATOR AND PHOTODETECTOR

The schematic of the MZ modulator is shown in Fig. 1. The optical waveguide is formed in the junction of a p-i-n diode. The epitaxial layers are grown on a (100) semi-insulating GaAs substrate. The intrinsic region consists of a 0.1-μm-thick layer of multiple quantum-well (MQW) layers sandwiched between two nominally undoped $Al_{0.05}Ga_{0.95}As$ layers of 0.4-μm thickness each. MQW layers are comprised of eight layers of 100 ÅGaAs/30 Å$Al_{0.27}Ga_{0.73}As$. A 1-μm-thick p (5×10^{17} cm^{-3} Be) $Al_{0.08}Ga_{0.92}As$ layers followed by a 1-μm-thick p^+ (2×10^{19} cm^{-3}C) $Al_{0.08}Ga_{0.92}As$ layer, and the lower cladding is a 2-μm-thick n (5×10^{17} cm^{-3}Si) $Al_{0.08}Ga_{0.92}As$ layer.

The phase-modulating electric signal, generating the electric field across MQW layers, propagates on a coplanar waveguide (CPW) along the optical waveguide. According to Kramers–Kronig relations, absorption spectrum variations of the MQW layers subject to the electric field modify the refractive index spectrum and, consequently, the phase of the optical wave. The propagation constant of the 50-Ω CPW is set to allow for the phase-modulating electric signal to travel in phase synchronism with the light. The output end of the device is terminated with 50-Ω resistors fabricated using a part of the waveguide semiconductor. The phase shift $\Delta\phi$ introduced into the optical mode is given by

$$\Delta\phi = \chi V_m L \frac{1 - e^{-\alpha L}}{\alpha L}(1 - \exp(-t/T_{\text{settling}})) \qquad (1)$$

1041-1135/$25.00 © 2008 IEEE

where χ is the phase modulation efficiency, V_m is the modulating electric voltage, L is the length of modulator, α is the microwave attenuation, and $T_{\rm settling}$ is given by [13]

$$T_{\rm settling} = 2.2\frac{d}{V} + 2\pi\frac{\rho\varepsilon}{d} + 2\pi L\frac{V_0 - V_c}{V_o V_c} \tag{2}$$

where d is the depletion region depth, V is the carrier average drift velocity across the depletion region, ρ is the p-i-n diode contact resistivity, and V_o and V_c are the velocities of the optical wave and the microwave, respectively.

Since the MQW layers are engineered to have an absorption band edge of 850 nm, optical absorption of signal beams with wavelengths somewhat longer than 850 nm can also be controlled through the QCSE [9] by applying large enough electric field across the MQW layers, thus allowing photodetectors with high absorption coefficients in the same layer structure. High-speed photodetector performance is achieved by carefully choosing the photodetector length and termination resistance.

III. Fabrication and Measurement

The GaAs–AlGaAs p-i-n layers are grown by molecular beam epitaxy on a semi-insulating GaAs substrate using Be and Si as p and n dopants. The semi-insulating GaAs substrate has the resistivity and thickness of $5.7 \times 10^8\ \Omega \cdot$cm and 250 μm, respectively. The 2-μm-wide ridge waveguides are defined by Cl reactive ion etching. A Au–Ni–Ge–Au n-contact metal region with total thickness of about 0.5 μm was formed by standard lift-off techniques and then rapid-thermal annealed at 415 °C for 30 s. A benzocyclobutene (BCB) layer was spun on the device and etched back to the top of the waveguide for planarization of the etched surface such that the CPW lines could be applied on the top. A Ti–Pt–Au evaporation and lift-off step forms metallization of the 1.5-mm-long CPW and the p-type metal contact. The widths of the center stripe and air gap of the integrated CPW line were 4 and 6 μm, respectively, to achieve a characteristic impedance of 50 Ω. The CPW 50-Ω termination is implemented by a 3-μm spacing between the active region and ground metal contacts.

By calculating the CPW propagation constant (Fig. 2) from scattering parameter measurements as a function of frequency an electric field settling time of 2.1 ps is estimated using (1, 2). Moreover, the expected operational bandwidth of the MZ modulator with this phase modulator in one arm is more than 50 GHz, where the microwave attenuation of the CPW is the primary bandwidth-limiting mechanism. It should be mentioned that the scattering parameters were measured for frequencies up to 50 GHz.

Fig. 3 illustrates the measured results of the interferometer's normalized output intensity as a function of the modulating input voltage at 870 nm and TE polarization. Low-frequency noise is filtered using a lock-in amplifier. An extremely low $V\pi$ of 0.45 V and a fairly high dc extinction ratio of 10 dB are achieved at 2-V reverse-bias. Moreover, the optical losses calculated from the MZ modulator dc characteristic shows an optical loss of 0.28 dBV$^{-1} \cdot$ mm^{-1} at 2-V modulator voltage.

The output intensity of the modulator was measured by a photodetector monolithically integrated in the interferometer output waveguide. The detector consists of a 400-μm active region, and the photocurrent is a function of MQW reverse bias. Leaving 6-μm spacing between the active region and ground metal contacts, equivalent to 100 Ω, provides a 50-Ω photodetector resistance. The combination 0.218-fF/mm parasitic capacitance along the photodetector active region and the 50-Ω termination resistance suggests a full-width at half-maximum (FWHM) pulsewidth of 5.5 ps for the 400-μm photodetector output.

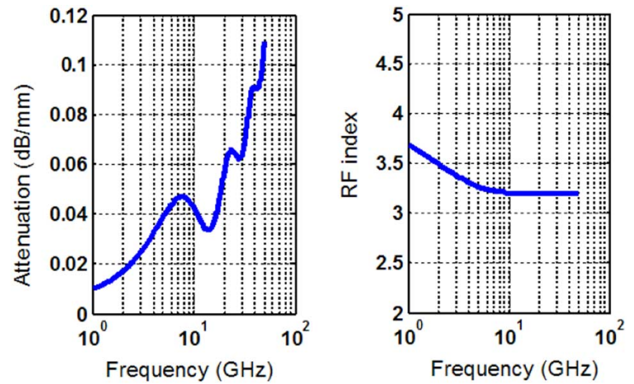

Fig. 2. CPW propagation constants.

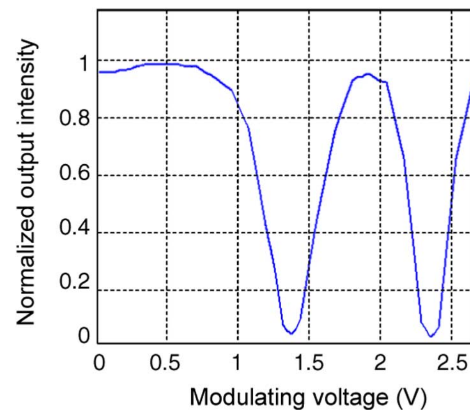

Fig. 3. MZ modulator output versus modulating voltage.

Fig. 4 shows the impulse responses of the photodetector measured by a pump–probe electrooptic sampling technique [14]. The 150-fs optical excitation pulses were obtained from a Ti : sapphire mode-locked laser at 870 nm. The measured response time and the estimated photodetector 3-dB bandwidth at 6-V reverse-bias is 8-ps FWHM and 33 GHz, respectively. Therefore, this photodetector is capable of detecting MZ modulations up to 33 GHz. Under intense illumination, the quantum efficiency of the photodetector degrades due to the electric field screening effect caused by the large number of photogenerated carriers. The saturation point, defined as the 1-dB compression of the quantum efficiency, is measured to be at an average optical power of 330 mW.

In order to investigate the small signal modulation bandwidth, the output of the MZ modulator in response to a 6-dBm sinusoidal input was monitored by a 20-GHz spectrum analyzer. Fig. 5 shows the output response at 2.1-V reverse-bias voltage. The interferometer output did not drop more than 3 dB over 1-

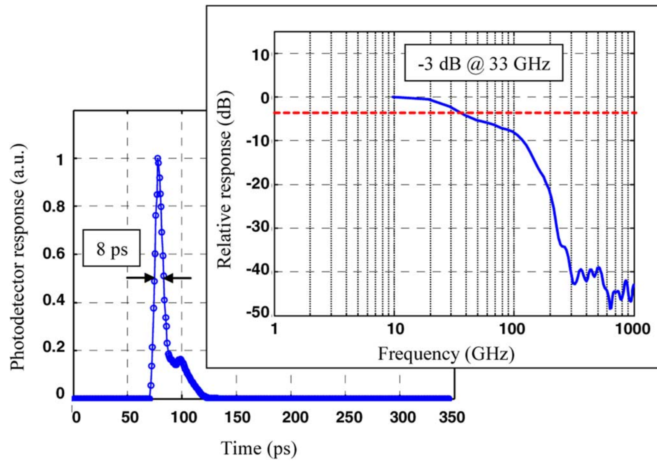

Fig. 4. Photodetector transient and frequency response.

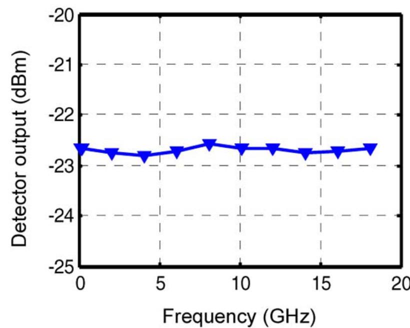

Fig. 5. Small signal modulation at 2.1-V bias.

to 18-GHz frequency range. Therefore, a measurement instrument-limited small signal bandwidth of more than 18 GHz is demonstrated for the phase modulator.

IV. Conclusion

MZ modulators for RF photonics are required to have low modulator driving voltages to allow for realistic circuit sizes, and sufficient bandwidth to operate at desired microwave frequencies. In this work, we have designed and fabricated a GaAs–AlGaAs MZ modulator, which achieves low drive voltage by utilizing QCSE-induced refractive index change along a relatively long modulator length and a high-speed modulation speed by employing a traveling-wave modulation scheme to relax the efficiency-bandwidth tradeoff. We obtained an extremely low driving voltage of 0.45 V for a signal-electrode of 1.5 mm at 870-nm wavelength. The measurement-instrument-limited small signal modulation bandwidth is measured to be 18 GHz, projected to an estimated bandwidth of 50 GHz. To our knowledge, this is the lowest reported MZ modulator driving voltage at such high modulation bandwidths.

Monolithically integrated photodetectors found in the same structure show an impulse response time of 8-ps FWHM, and saturation power of 330 mW.

Acknowledgment

The authors wish to acknowledge Prof. R. F. W. Pease for discussions and advice in this work, and Prof. Y. Nishi. Special thanks go to H. Chin and O. Fidaner for help with the measurement setup, and D. Mars, Agilent Technologies, for wafer growth.

References

[1] A. Narasimha, B. Analui, L. Yi, T. J. Sleboda, and C. Gunn, "A fully integrated 4×10 Gb/s DWDM optoelectronic transceiver in a standard 0.13 μm CMOS SOI," in *Int. Solid State Circuits Conf. 2007 Dig. Tech. Papers*, 2007, pp. 570–571.

[2] D. A. B. Miller, A. Bhatnagar, S. Palermo, A. Emami-Neyestanak, and M. A. Horowitz, "Opportunities for optics in integrated circuits applications," in *Int. Solid State Circuits Conf. 2005 Dig. Tech. Papers*, pp. 86–87.

[3] J. Chou, Y. Han, and B. Jalali, "Adaptive rf-photonic arbitrary waveform generator," *IEEE Photon. Technol. Lett.*, vol. 15, no. 4, pp. 581–583, Apr. 2003.

[4] M. Khodier, G. Tzeremes, T. S. Liao, P. K. L. Yu, and C. G. Christodoulou, "Smart RF/photonic antennas for ultra high capacity wireless communications," in *Proc. SPIE Digital Wireless Commun. IV*, 2002, vol. 4740, pp. 132–141.

[5] H. R. Fetterman, S. R. Forrest, and D. V. Plant, "Optical controlled phased array radar receivers," in *Antennas Propagation Soc. Int. Symp.*, Ann Arbor, MI, Jun. 28–Jul. 2, 1993.

[6] H. Zmuda *et al.*, "Optically assisted high-speed, high resolution analog-to-digital conversion," *Proc. SPIE*, vol. 5814, pp. 51–61, 2005.

[7] M. Sugiyama, M. Doi, S. Taniguchi, T. Nakazawa, and H. Onaka, "Driver-less 40 Gbit/s $LiNbO_3$ modulator with sub-1 V drive voltage," in *Proc. Opt. Fiber Commun. Conf.*, May 2002, pp. 853–856.

[8] M. Jarrahi, D. A. B. Miller, R. F. W. Pease, and T. H. Lee, "Optical spatially quantized high performance analog-to-digital conversion," in *Proc. Conf. Lasers Electro-Optics (CLEO)*, Baltimore, MD, May 6–11, 2007, Paper CWJ7.

[9] D. A. B. Miller, D. S. Chemla, T. C. Damen, A. C. Gossard, W. Wiegmann, T. H. Wood, and C. A. Burrus, "Electric field dependence of optical absorption near the bandgap of quantum-well structures," *Phys. Rev. B*, vol. 32, no. 2, pp. 1043–1060, Jul. 15, 1985.

[10] J. S. Weiner, D. A. B. Miller, and D. S. Chemla, "Quadratic electro-optic effect due to the quantum-confined Stark effect in quantum wells," *Appl. Phys. Lett.*, vol. 50, pp. 842–844, 1987.

[11] D. Jager and R. Kremer, "Traveling-wave optoelectronic devices for microwave application," in *Proc. Int. 1994 IEEE MTT-S Topical Meet. Opt. Microwave Interactions*, Nov. 21-23, 1994, pp. 11–14.

[12] T. H. Wood, J. Z. Pastalan, C. A. Burrus, Jr., B. C. Johnson, B. I. Miller, J. L. de Miguel, U. Koren, and M. G. Young, "Electric field screening by photogenerated holes in multiple quantum wells: A new mechanism for absorption saturation," *Appl. Phys. Lett.*, vol. 57, pp. 1081–1083, 1990.

[13] L. Y. Lin, M. C. Wu, T. Itoh, T. A. Vang, R. E. Muller, D. L. Sivco, and A. Y. Cho, "High-power high-speed photodetectors-Design, analysis, and experimental demonstration," *IEEE Trans. Microw. Theory Tech.*, vol. 45, no. 8, pp. 1320–1331, Aug. 1997.

[14] K. J. Weingarten, M. J. W. Rodwel, and D. M. Bloom, "Picosecond optical sampling of GaAs integrated circuits," *IEEE J. Quantum Electron.*, vol. 24, no. 2, pp. 198–220, Feb. 1988.